JACS
JOURNAL OF THE AMERICAN CHEMICAL SOCIETY

Article

The impact of aromatic stacking on glycoside reactivity: balancing CH/# and cation/# interactions for the stabilization of glycosyl-oxocarbenium ions

Laura Montalvillo-Jiménez, Andrés G. Santana, Francisco Corzana, Gonzalo Jiménez-Osés, Jesús Jiménez-Barbero, Ana M. Gomez, and Juan Luis L. Asensio

J. Am. Chem. Soc., **Just Accepted Manuscript** • DOI: 10.1021/jacs.9b03285 • Publication Date (Web): 07 Aug 2019

is published by the American Chemical Society. 1155 Sixteenth Street N.W., Washington, DC 20036

The impact of aromatic stacking on glycoside reactivity: balancing CH/π and cation/π interactions for the stabilization of glycosyl-oxocarbenium ions

Laura Montalvillo-Jiménez,[‡a] *Andrés G. Santana,*[‡a] *Francisco Corzana,*[b] *Gonzalo Jiménez-Osés,*[c] *Jesús Jiménez-Barbero,*[c,d] *Ana M. Gómez,*[a] *Juan Luis Asensio*[a]*

[a]Instituto de Química Orgánica (IQOG-CSIC), Juan de la Cierva 3, 28006 Madrid, Spain. Fax: +34-91-5644853; Tel: +34-91-5622900.

[b]Dept. Química and Centro de Investigación en Síntesis Química, Universidad de La Rioja.

[c]Center for Cooperative Research in Biosciences (CIC-bioGUNE).

[d]Basque Foundation for Science, Ikerbasque.

‡ **AGS and LM-J are both first authors**

* e-mail: juanluis.asensio@csic.es, phone: +34 915622900, Fax: +34 915644853

ABSTRACT

Carbohydrate/aromatic stacking represents a recurring key motif for the molecular recognition of glycosides, either by protein binding domains, enzymes or synthetic receptors. Interestingly, it has been proposed that aromatic residues might also assist in the formation/cleavage of glycosidic bonds by stabilizing positively charged oxocarbenium-like intermediates/transition states through cation/π interactions. While the significance of aromatic stacking on glycoside recognition is well stablished, its impact on the reactivity of glycosyl donors is yet to be explored. Herein, we report the first experimental study on this relevant topic. Our strategy is based on the design, synthesis and reactivity evaluation of a large number of model systems, comprising a wide range of glycosidic donor/aromatic complexes. Different stacking geometries and dynamic features, anomeric leaving groups, sugar configurations and reaction conditions have been explicitly considered. The obtained results underline the opposing influence exerted by van der Waals and coulombic forces on the reactivity of the carbohydrate/aromatic complex: depending on the outcome of this balance, aromatic platforms can indeed exert a variety of effects, stretching from reaction inhibition all the way to rate enhancements. Although aromatic/glycosyl cation contacts are highly dynamic, the conclusions of our study suggest that aromatic assistance to glycosylation processes must indeed be feasible, with far reaching implications for enzyme engineering and organocatalysis.

INTRODUCTION

Aromatic stacking plays a prominent role in the molecular recognition of saccharidic ligands by proteins, nucleic acids or synthetic receptors.[1-3] These contacts result from a combination of dispersive, hydrophobic and electrostatic forces, involving polarized pyranose CH groups and the aromatic electronic quadrupole,[4,5] and can exhibit a variety of geometries. Their relevance is highlighted by data-mining studies which show the extraordinary high frequency of aromatic amino acids, especially tryptophan, in the carbohydrate binding sites of proteins. Of note, tryptophan, tyrosine and phenylalanine residues are also common within the catalytic sites of glycosidases and glycosyl transferases, prompting the question of whether they might also assist the cleavage or formation of glycosidic bonds (Figure 1).

Different scenarios can be envisaged to describe the influence of aromatic stacking on the reactivity of pyranoses. Thus, for concerted S_N2 processes, shielding of the anomeric center by the aromatic platform would be expected to exert a protective influence, potentially leading to a sharp decrease in reactivity. On the contrary, more dissociative transition states might benefit from favorable electrostatic forces arising between the aromatic quadrupole and the pyranose developing positive charge (cation/π interaction), [6,7] especially in low dielectric environments (Figure 1). In addition, aromatic/glycosyl cation interactions could be expected to drive the stereochemical course of the reaction by preventing the nucleophilic attack through either the α or β pyranose face. Fittingly, oxocarbenium-like intermediates or transition states have commonly been invoked to explain the outcome of glycosylation and glycoside hydrolytic reactions both in the chemical[8-12] and enzymatic contexts.[13-15] As a further consideration, the formation of glycosyl cations is usually accompanied by substantial conformational changes of the reactive pyranose ring.[8] Conceivably, this geometric adjustment could be impeded, or facilitated, by pre-organized CH/π bonds, depending on the interaction geometry and dynamic behavior of the complex. Additional factors such as the access of solvent molecules to the catalytic region, its local dielectric enviroment or the presence of counter ions should also be taken into account, drawing a rather complex scenario. In fact, while the relevance of aromatic platforms in glycan recognition is undisputable, their possible roles in catalysis remain uncertain.

Despite the relative lack of experimental information available on this topic, some examples have been reported in which tyrosine or phenylalanine residues seem to assist the cleavage/formation of glycosidic linkages by presenting favourable interactions with the carbohydrate transition states. Thus, a *hydrophobic platform* comprising a phenylalanine residue, highly conserved in the active centre of *all* glycosyl hydrolases, has been proposed as a *mechanistically relevant transition state stabilising factor*.[16] More recently, a seminal contribution by Davis and col. has put forward a novel mechanism for a 'S_Ni synthase', engineered from a retaining 'double-S_N2' hydrolase.[17] According to kinetic, structural and theoretical considerations, this mutant protein makes use of a tyrosine residue,

instead of a carboxylate, to stabilize the oxocarbenium-like transition state generated during the front-face attack of the glycosidic acceptor to the acetalic center (Figure 1b). Interestingly, this tyrosine residue is originally involved in a parallel stacking with the α-face of the glycosidic donor and therefore seems to play a dual role, participating both in substrate recognition and catalysis. These examples illustrate that under appropriate conditions, aromatic platforms can be employed to stabilize glycoside transition states. However, the precise structural and chemical requirements for this function are presently unknown.

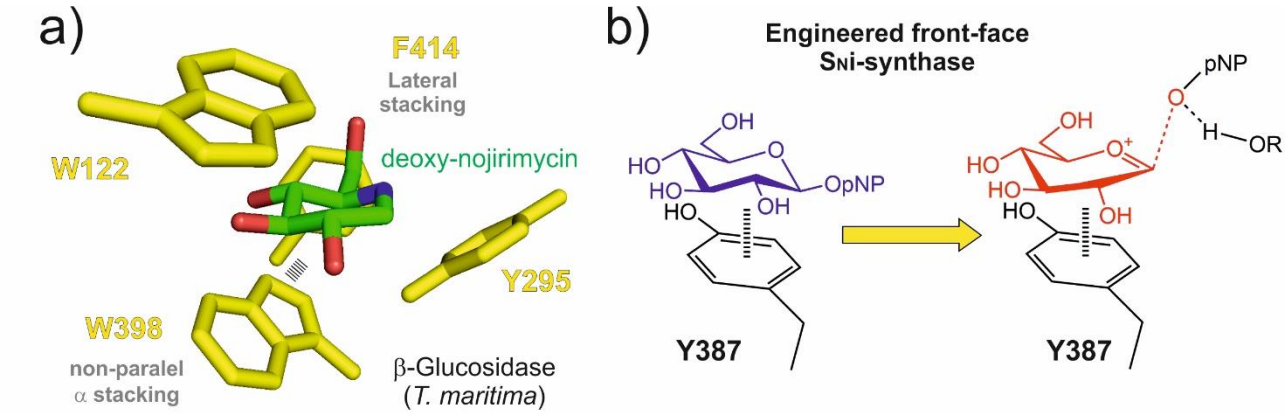

Figure 1.-*a) Aromatic interactions in a β-glucosidase/DNJ complex as revealed by the corresponding X-ray diffraction structure (pdb code: 2J77) . b) Aromatic assistance promotes catalysis in the context of an engineered front-face S_Ni-synthase.*[17]

Our aim is to understand the influence of carbohydrate/aromatic stacking on the pyranose reactivity to eventually apply this knowledge for synthesis and catalysis. With this purpose in mind, and as a first step, we have herein employed a chemical approach based on the design, synthesis and evaluation of appropriate molecular systems, in conjunction with the extensive use of NMR as a key monitorization and detection tool, facilitated in particular cases by the employment of ^{13}C-labeled models. Despite its significance, both from the fundamental and applied perspectives, this work represents, to the best of our knowledge, the first systematic experimental study reported on this topic.

RESULTS

a) Design of the model glycosidic-donor/aromatic complexes: Basic principles. – In order to enhance any potential stabilizing electrostatic interaction between the aromatic quadrupole and the cationic intermediates/transition states, we decided to carry out our studies in a low dielectric environment such as chloroform (ε=4.8).[18] It is worth mentioning that comparable dielectric constants have been previously theorized to properly model the inner protein environment in binding sites or catalytic regions.[19] Accordingly, the designed scaffolds encompass pyranose units equipped with several non-participating MeO- groups, which in turn provide high solubility in organic solvents.

Two alternative families of model systems were conceived (Figure 2a). Compounds in family I contain a disaccharide scaffold. The reactive pyranoses display alternative leaving groups at the

anomeric centre and participate in contacts with a pyrene platform that is attached to a vicinal 3-amino-allose unit through an amide bond (compounds **1**-**3**, **6** and **8**). Alternatively, the compounds in family II (Figure 2b) include a glycosyl donor involved in a stacking complex with a pyrene unit that is tethered to a 4,6-*O*-benzylidene protecting group. Considering the key influence exerted by the chemical nature and presentation of the substituent at position 2 of the pyranose moiety on the reactivity of the acetalic center, manno- (**10**) gluco- (**11**) and 2-deoxy-gluco- (**16**) derivatives were explicitly considered. Moreover, to maximize the influence of the aromatic ring on the pyranose behavior, a derivative comprising a 2-deoxy-glucose donor sandwiched between two pyrene platforms was also prepared (**18**). For comparison purposes, both families include reference compounds equipped with smaller or non-aromatic units (derivatives **4**, **5**, **7** and **9** for type I models and **12**-**15**, **17** and **19** for type II models). Finally, selected type II models were also prepared incorporating ^{13}C atoms, either at all pyranose positions (**11**, **14**, **15**, **16** and **17**) or just at the anomeric center (**10** and **13**). Thus, relatively fast reactions could be conveniently monitored using 2D HSQC NMR experiments, also allowing an easy and sensitive detection of the transient species even in highly overlapped spectra (see the experimental section).

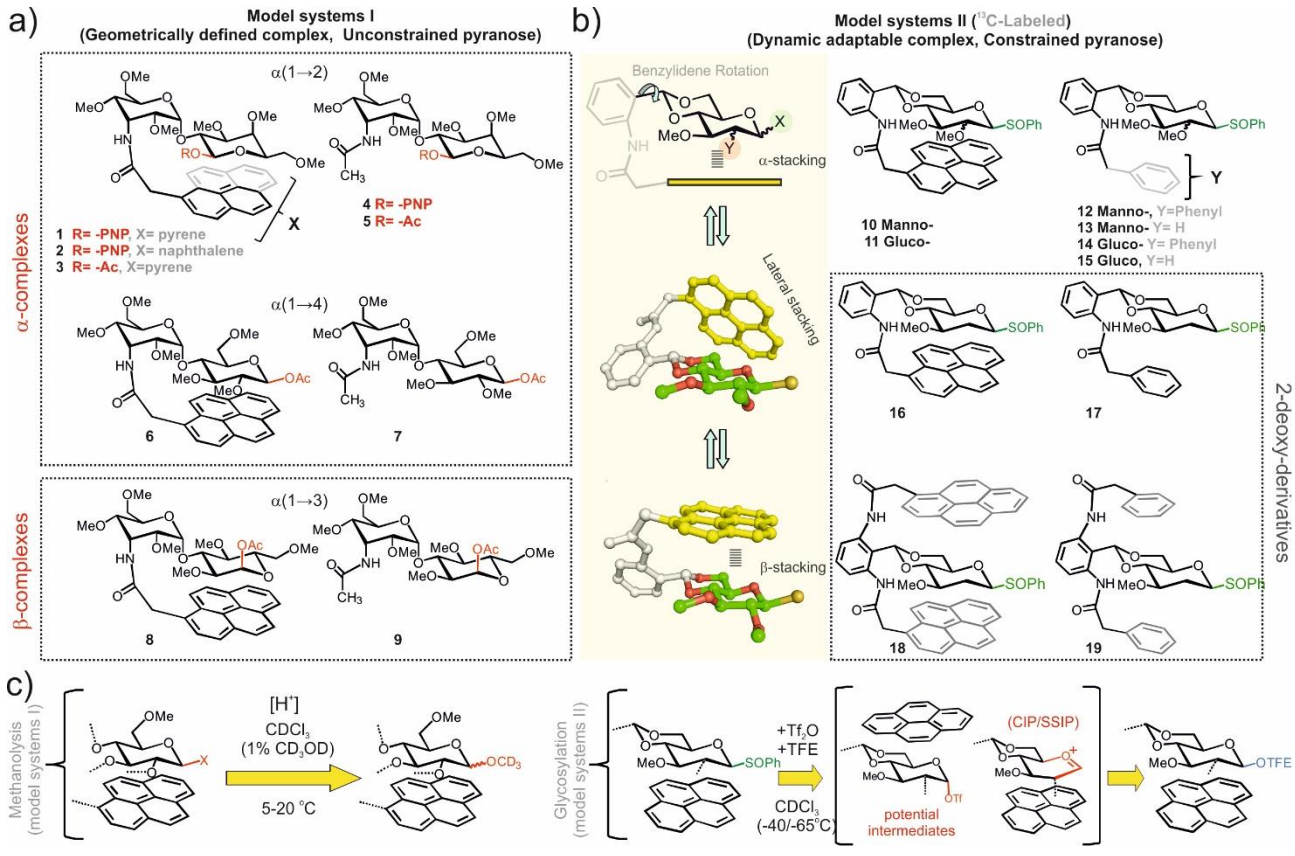

Figure 2.- *Chemical structures of model systems I (a) and II (b). Conformational variability for the established carbohydrate/aromatic complexes type II is illustrated. c) Chemical reactions selected to evaluate the impact of aromatic stacking on glycoside reactivity. CIP and SSIP stand for close ion pair and solvent-separated ion pair, respectively.*

There are two important differences between models type I and II that are relevant from a reactivity perspective and deserve special attention. First, family I scaffolds generate stable

carbohydrate/aromatic complexes with a defined geometry, involving either the α- (**1**-**3**, **6**) or the β- (**8**) face of the pyranose (Figure 2a). On the contrary, for type II systems, rotation of the benzylidene moiety with respect to the pyranose unit is allowed. This fact provides a highly dynamic environment to form adaptable carbohydrate/aromatic stacking complexes. Indeed, MD simulations confirm that several interaction geometries are possible for these type II systems. They comprise parallel and parallel-shifted complexes mediated by the α- or β face of the glycoside, together with lateral, edge-to-face aromatic stacking modes involving the hydroxymethyl moiety (Figure 2b and S1). As a second consideration, family I derivatives encompass an unconstrained pyranose donor, while for family II, the pyranose units are fixed by the 4,6-*O*-benzilidene moiety. Consequently, only a reduced subset of the pyranose conformational space is available for the oxocarbenium-like transition states/intermediates. The resulting combinations (fixed stacking/flexible pyranose, in models type I and adaptable stacking/constrained pyranose, in models type II) allow dissecting the influence of aromatic stacking on the glycoside reactivity in two complementary scenarios.

The anomeric leaving groups for both scaffolds were selected based on chemical considerations (Figure 2c). Family I derivatives are structurally more complex and more challenging to obtain with ^{13}C-labels. Therefore, they were tested in straightforward acid-catalyzed methanolysis reactions, for which acid labile *p*-nitro-phenoxy or acetoxy anomeric substituents were incorporated at the reactive site. These processes are assumed to proceed through cationic transition states.[9] On the other hand, family II scaffolds afforded less overlapped NMR spectra. The use of ^{13}C-labels for particular models offered the opportunity to carry out more demanding, low temperature assays with relevant glycosylation reaction conditions.[8] Accordingly, these models displayed phenyl sulfoxide moieties as leaving groups. Such glycosylations proceed through a continuum of mechanisms spanning the gap between pure S_N2 and S_N1 processes, as shown by extensive studies performed by Crich and col.[8] These reactions require the participation of several key intermediates (Figure 2c), including glycosyl triflates[20] and/or glycosyl oxocarbenium ions (either solvent equilibrated or forming close ion pairs with the corresponding counterions).[8] Fortunately, more dissociative processes, involving cationic transition states, can also be favoured by the appropriate choice of the acceptor alcohol, as recently shown by Codée and col.[21] Taking these factors into account, we selected a weakly nucleophilic acceptor such as trifluoroethanol (TFE), unless stated otherwise.

b) General synthetic strategy. - The synthetic route for the preparation of all systems is represented in Scheme 1. The glycosylation reaction between a glycosyl donor containing a phenyl 3-azido-3-deoxy α-D-*allo*-thiopyranoside unit[5b] and the appropriately protected glycosyl acceptor (2-OH-*galacto*-, 3-OH-*gluco*-, and 4-OH-*gluco*-pyranosides, containing a leaving group at the anomeric position from which the oxocarbenium ion could be generated) [22] gave the desired (α1→2)-, (α1→3)- and (α1→4)-linked disaccharides. The subsequent steps included the Staudinger reduction of the azide moiety followed by amide coupling with the corresponding (aryl)acetic acid to grant access to

model sytems type I, **1-9**. In a similar manner, 4,6-*O*-benzylidenation of thioglycosides (gluco-, manno- and 2-deoxy-gluco-) with the appropriate arylaldehyde dimethylacetal, followed by the analogous Staudinger reduction/amide coupling sequence provided the target constrained pyranose type II systems, **10-19**. A detailed description of the synthetic protocols, together with the characterization of products and intermediates, is included in the supplementary material.

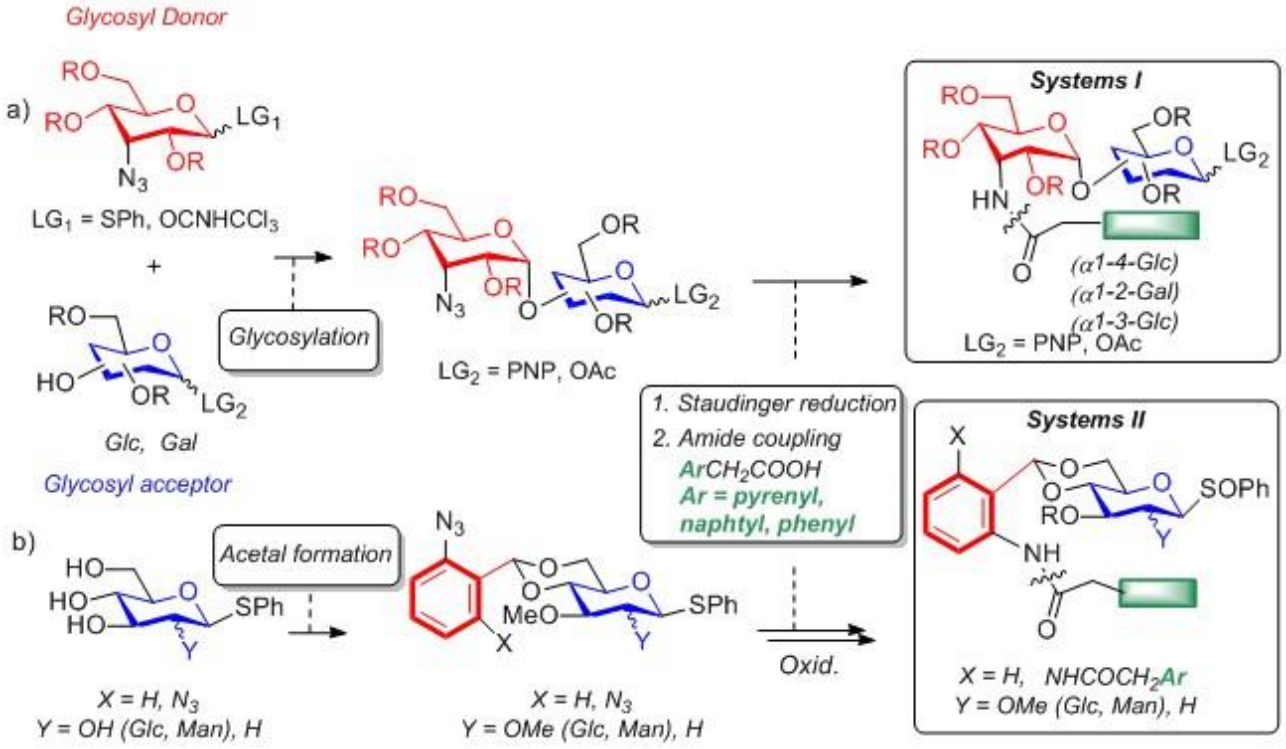

***Scheme 1**. General synthetic route for the model systems I and II.*

c) Reactivity evaluation of family I systems: methanolysis reactions.- Once the synthesis of the target models was successfully accomplished, we proceeded to verify the formation of the anticipated carbohydrate/aromatic complexes in solution. Satisfactorily, obtained results for **1-9** were in accordance with the design principles previously outlined. As an example, the NMR data for **1** were consistent with the formation of a well-defined complex involving the pyrene platform and the α-face of the reactive unit. Thus, HSQC signals for Gal H1, H3 and H5 appear extremely up-field shifted in the ^{1}H dimension (Figure 3a, left and S1), highlighting their direct involvement in strong CH/π bonds with the aromatic unit. To reveal the impact of such interaction pattern on the pyranose reactivity, the methanolysis of compound **1**, and the corresponding references **2** and **4**, was monitored using 2D-HSQC experiments in deuterated chloroform at 20 ºC (Figure 3a-c). Interestingly, the addition of 1 μl of triflic acid to a solution of disaccharide **1** in the absence of acceptor alcohol led to an extreme broadening of the NMR signals, consistent with the presence of several species in the intermediate exchange regime on the NMR chemical shift time-scale. Quenching of this sample with 5 μL of CD_3OD yielded a major product, with no carbohydrate/aromatic stacking, as judged from the observed chemical shift data. This derivative proved to be extremely unstable, rendering all isolation efforts fruitless. Fortunately, both NMR and mass spectrometry analyses of the reaction mixture

provided key structural information, strongly suggesting the formation of the highly strained macrocyclic *C*-glycoside shown in Figure 3a (see also Figure S2). Thus, the Gal anomeric carbon (with a broad peak at δ_C 80 ppm) presented non-ambiguous HMBC and NOE correlations with the pyrene unit. Moreover, the measured $^3J_{HH}$ coupling constants were still fully consistent with a $^4C_1$ conformation for both pyranose units. More intriguingly, the final *C*-glycoside exhibits a β-configuration as shown by its $^3J_{H1\text{-}H2}$ coupling constant (9.5 Hz). This was totally unanticipated from the structure of the original carbohydrate/pyrene complex (with the aromatic unit stacked on the α-face of the galactose), suggesting that formation of the glycosyl cation is followed by a significant conformational rearrangement (Figure 3a).

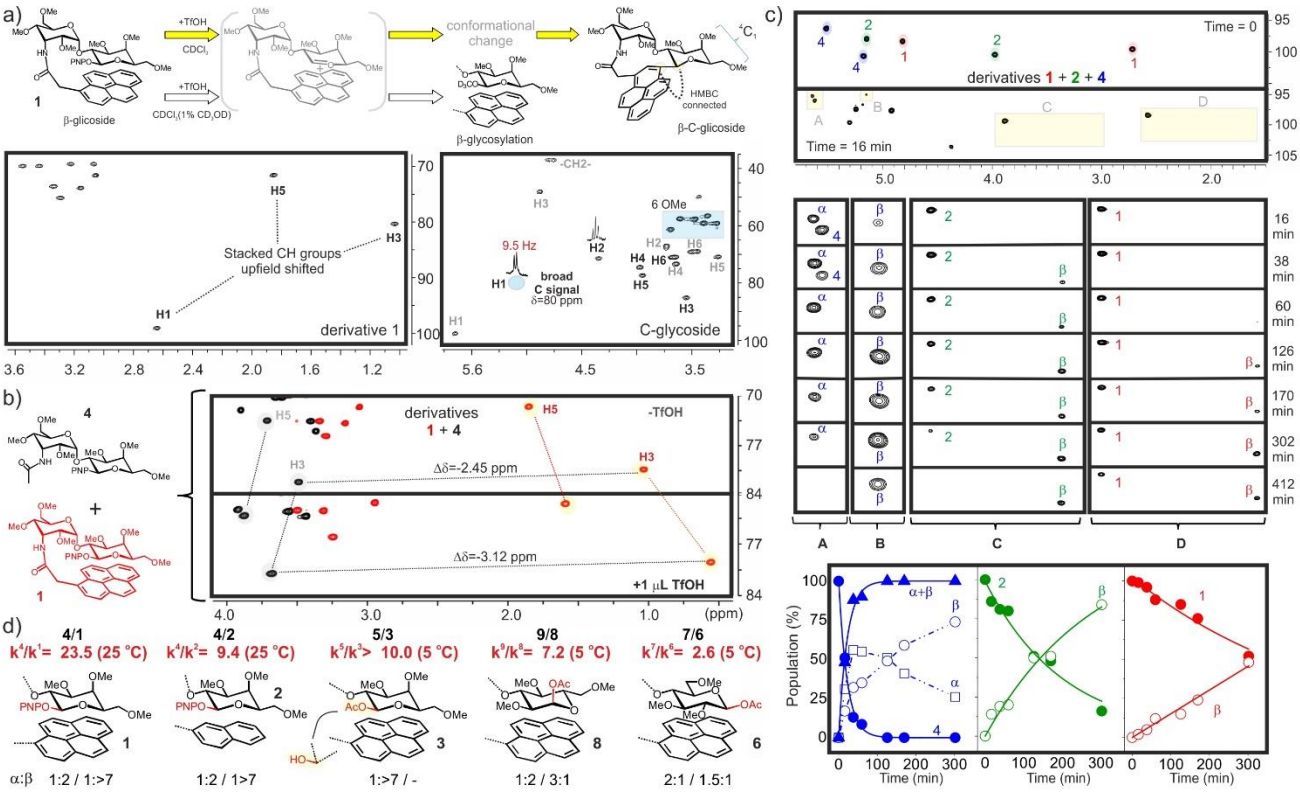

Figure 3.-*Family I. a) Top.- Chemical evolution of **1** upon treatment with triflic acid, both in the absence and presence of 1% CD_3OD. Bottom.- Key region of the HSQC NMR spectra recorded for **1**, along with the proposed C-glycosidic structure. b) HSQC spectra of a **1**(red)/**4**(black) mixture before and after triflic acid addition. Δδ values (ppm) for representative signals are indicated. c) Reactivity assays with a **1**(blue)/**2**(green)/**4**(red) equimolecular mixture in $CDCl_3$ (1% CD_3OD) at 25 °C. Top.- Initial data sets (anomeric region). Middle.- Insets A-D (highlighted with yellow boxes above) at different times. Bottom.- Reaction profiles derived from the integration of anomeric cross-peaks. d) Kinetic constant ratios measured for **1**-**3**, **6** and **8** with respect to the corresponding reference derivatives. The resulting anomeric α:β ratios are also shown.*

In contrast, the addition of 4 μL of triflic acid in the presence of 1% CD_3OD triggers a smooth methanolysis process, which can be conveniently monitored by NMR. Interestingly, this protocol leads to partial protonation of the disaccharides, with opposite behaviors for the pyrene-bearing compounds and the reference derivatives. As an example, Figure 3b displays the HSQC spectra acquired for an equimolecular mixture of **1** (red) and **4** (black) in the absence and presence of TfOH

(1 μL). It can be observed that the acidic conditions induce slight down-field shifts in the NMR signals of model **4**. On the contrary, for **1** those protons already involved in CH/π interactions with the aromatic platform are shielded even further. As a consequence, the chemical shift perturbations promoted by aromatic stacking on the reactive pyranose unit (with respect to reference compound **4**, see Figure 3b) are significantly enhanced, reaching unusual values even larger than $\Delta\delta > 3$ ppm. In conclusion, partial protonation of the reactive pyranose turns the original CH/π interactions into a much stronger cation/π interaction leading to a significant stabilization of the carbohydrate/aromatic complex. A similar behavior was observed for all the stacking complexes tested regardless of the pyranose interacting face (α or β), as gathered in Figure 3b and S3-S6.

The chemical evolution of an equimolecular mixture of **1**, **2** and **4**, upon the addition of triflic acid is represented in Figure 3c. The integration of the relevant reagent and product cross-peaks with time allowed to build a reaction time-course for each of the three derivatives assayed. According to these data, reference **4**, for which no aromatic unit is present, rapidly evolves to yield a mixture of methyl α- and β-*O*-glycosides with a half-reaction time ($t_{1/2}$) ca. 15 min. A slower methanolysis process is apparent for **1** and **2**, containing a pyrenyl and naphthyl residue ($t_{1/2}$ values of 353 and 140 minutes, respectively). Interestingly, in these latter cases a single β methyl glycoside product was detected. Reaction time-courses were translated into kinetic constants assuming pseudo-first order conditions. Then, the influence of aromatic stacking on reactivity was expressed in terms of kinetic constant ratios ($k^{reference}/k^{+aromatic}$). Employing this general protocol, the rest of family I model systems were tested. The obtained results are summarized in Figure 3d and reveal a consistent inhibition of the glycoside reactivity by the presence of aromatic stacking. Indeed, these reactivity falls are in the 2- to 20-fold range, depending on the strength and geometry of the original carbohydrate/aromatic interaction. Significantly, this effect is, in some cases, accompanied with an increase in the stereoselectivity of the process, which is particularly clear for the strongest/less reactive complexes. For example, methanolysis of the reference compound **4** produces an initial 2:1 α:β mixture that equilibrates to the final 1:2 ratio observed under these acidic reaction conditions. On the contrary, donor **1**, which is involved in a strong stacking complex with the pyrene unit, yields only the retention β-product. This observation is in accordance with the behavior recently described for an engineered S_Ni-synthase (Figure 1b)[17] and might also point to an S_Ni mechanism for this particular substitution process.

In summary, according to the obtained data, the aromatic systems in family I models exert a preferential stabilization of the ground state and partially charged pyranoses over the oxocarbenium-like transition state, leading to a net increase in the global activation energy of the process. This conclusion is consistent with the apparent strength of the observed CH/π contacts, specially under

acidic conditions (as judged by Δδ values) and suggests that the geometric and dynamic properties of the initial complex are of critical importance for reactivity.

d) Reactivity evaluation of family II systems: low-temperature glycosylations. **-** With these results in hand, we decided to explore the influence of the pyrene unit in a rather different context (Figures S7-S21). As previously mentioned, type II molecules combine more dynamic carbohydrate/aromatic interactions with a conformationally constrained reactive pyranose. Indeed, the transient dynamic character of the CH/π bonds is now reflected in the reduced chemical shift perturbations (Δδ< 2 ppm for **10**, **11** and **16** even at temperatures below -50 ºC) promoted by the aromatic systems at the sugar unit.

Reactivity assays were individually performed for **10**-**19** at temperatures in the -65/-50 ºC range and monitored by 1D and/or 2D-HSQC NMR experiments, employing regular or ^{13}C-labeled molecules (Figures 4-6).[22] As internal standard for integrations, an equimolecular amount of 4,4,5,5-tetramethyl-2-(1-naphthalenyl)-1,3-dioxolane was included in the reaction mixtures.[23] Considering the increased complexity of these multi-component reactions, a minimum of three runs, under identical reaction conditions, were completed for every case. Pairwise competition experiments were also carried out for qualitative comparison purposes. In all cases, glycosyl donors were activated with triflic anhydride in the presence of 5-8 equivalents of TFE depending on the model compound, as described in the experimental section.

The mannose case.- The major conformation of **10** is represented in Figure 4a and displays a preferred stacking geometry that involves the α-face of the mannose unit, as shown by the chemical shift data (Figure S8). The glycosylation reactions furnished a mixture of products (**20**α and **20**β) with a 70-80% overall yield (Figure S9), slightly lower than those obtained from the reference compounds **12** and **13** (75%-85%). Unexpectedly, the stereoselectivity of the process vanishes in the presence of the pyrene system (from 1:4 to 1:1).

NMR experiments performed both with individual donors and equimolecular **10**/**13** ^{13}C-labeled mixtures allowed us to estimate the relative **20** (α/β) and **22** (α/β) concentrations at short reaction times (5-10 min). The obtained values, which are proportional to the relative formation rates, are represented as a bar chart in Figure 4c (see also Figure S10). According to these data, the aromatic stacking has an opposite effect on the individual product formation rates: two-fold increase for the α-anomer and 2-fold decrease for the β-derivative, consistent with the observed degradation of the stereoselectivity. Interestingly, even in the presence of five equivalents of TFE, the α-glycosyl triflates formed from both **10** and **13** were detected throughout the reaction and displayed comparable steady concentrations. This behavior reflects the higher nucleophilic character of the triflate anion with respect to TFE or to the aromatic unit itself.[8,24] It should be noted that the formation the of an α-triflate from **10** requires a rearrangement of the initial carbohydrate/aromatic complex, which is

greatly facilitated by the adaptable nature of the designed scaffold. Indeed, the pyrene unit swings from the mannose α-face to a lateral disposition, establishing CH/π bonds with the hydroxymethyl moiety, whose protons are now shielded up to Δδ= -1.7 ppm. These intermediates were also characterized by NMR employing a pre-activation protocol, as shown in Figure S8. A similar outcome was obtained employing **10**/**12** mixtures (Figure S11). These unexpected results prompted us to further interrogate alternative aromatic/donor complexes also belonging to family II.

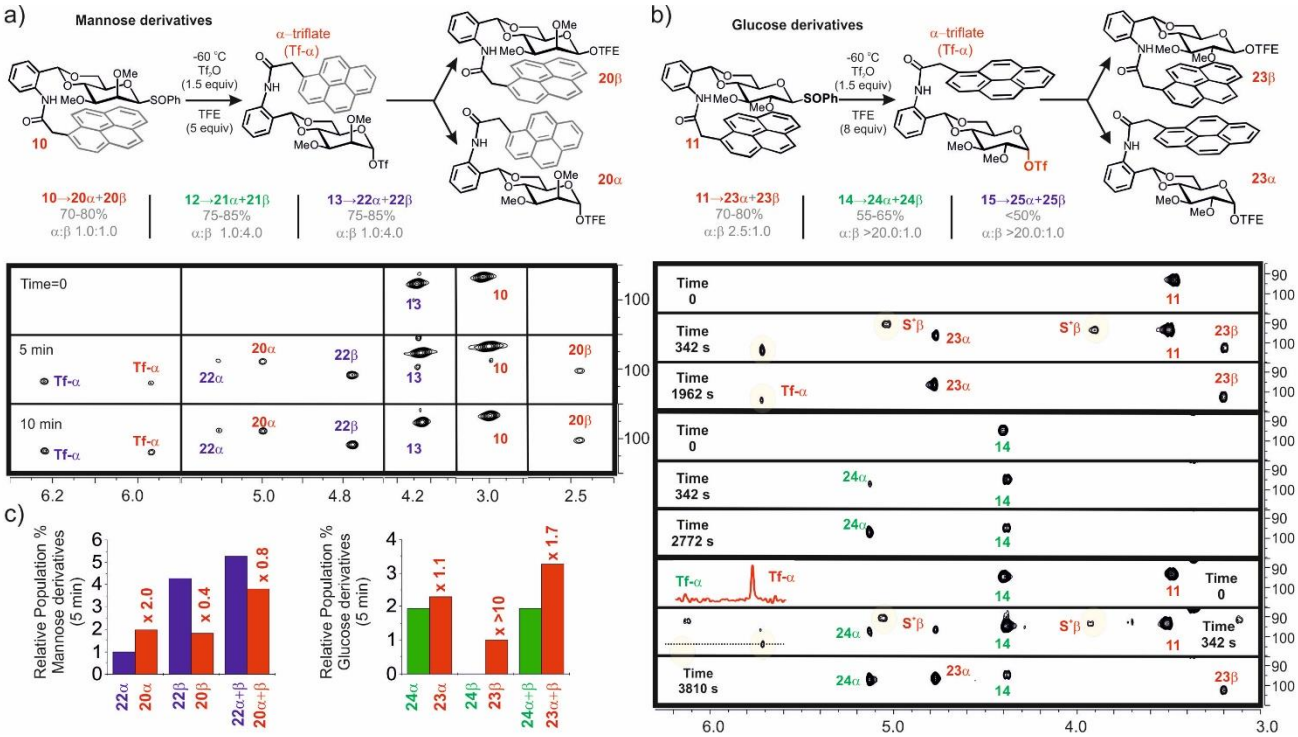

Figure 4.- *Family II. a) The mannose case. Glycosylation of **10** with TFE. Yields and stereoselectivities obtained from **10**, **12** and **13** are shown below. Representative HSQC regions of the NMR-based competition experiment (-60 °C) carried out with an equimolecular ^{13}C-labeled **10**/**13** mixture at three different reaction times are displayed. b) The glucose case. Glycosylation of **11** with TFE. Yields and stereoselectivities obtained from **11**, **14** and **15** are shown below. Representative HSQC regions of glycosylations (-60 °C) performed with ^{13}C-labeled **11** (top), **14** (middle) and a **11**/**14** mixture (bottom) at three different reaction times are displayed. c) Bar charts represent the observed relative populations for the corresponding products at short reaction times.*

The glucose case.- β-glucopyranosyl sulfoxide **11** exhibits a highly dynamic conformational behavior, as deduced from the significant chemical shift perturbations observed for the ^{1}H NMR resonances for both pyranose faces. MD simulations also supported the co-existence of α- and β-stacking complexes in equilibrium (Figures S1 and S12-S14). Glycosylations with donors **11**, **14** and **15** (see also Figures S15-S17) revealed a significant effect of the pyrene unit on the observed stereoselectivity, which decreased from >20:1 to 2:1, although with an overall improvement of the reaction yield. The use of ^{13}C-labeled donor molecules allowed to pinpoint further reactivity differences between **11** and the reference derivatives **14** and **15**. Thus, for the pyrene-stacked donor **11**, the process proceeds with a substantial accumulation of three transient activated species: an α-

glycosyl triflate and two unidentified β-species, marked as $S^{+}\beta$ in Figure 4b. Their ^{13}C NMR chemical shifts and heteronuclear $^{1}J_{HC}$ constant values (168 Hz) strongly point at sulfonium species. On the contrary, analogous intermediates were barely detectable in the absence of a stacked aromatic unit (**14** and **15**). Of note, the triflate formed from **11** presents clear CH/π interactions with the pyrene platform, which in this case are mediated by the pyranose β-face CH groups. This transient triflate species was also prepared following a pre-activation protocol, which allowed its unambiguous characterization (Figure S14). Regarding the reaction kinetics, both individual assays and competition experiments revealed that the formation rate of the major α-stereoisomer is marginally increased by the presence of the pyrene unit (Figure 4b, **23**α vs **24**α), while that of the minor β-anomer is much more enhanced, as represented in Figure 4c (bar chart). This fact accounts for the observed stereoselectivity.

As a final point, the larger accumulation of intermediate species formed from **11** indicates that their formation and/or consumption rates must be significantly altered by the existence of the carbohydrate/aromatic stacking. Fittingly, pre-activation experiments (Figure S18-S19) confirmed that triflate formation is significantly accelerated in the presence of the pyrene unit, strongly suggesting the presence of a transition state with a significant cationic character for this step.

The 2-deoxy-glucose case.- Among common glycoside donors, 2-deoxy-derivatives, lacking an electron-withdrawing substituent at the neighboring position to the anomeric center, present the highest tendency to evolve through dissociative, more cationic transition states.[25] This fact ensures a S_N1-like behavior even when nucleophilic alcohols are considered. Accordingly, for the reactivity analysis of these models, monofluoroethanol (MFE) was incorporated as an additional acceptor.

NMR reactivity experiments performed with ^{13}C-labeled models revealed, in all cases, a clean evolution from reagents to products, with no detectable intermediates, which is consistent with the higher reactivity expected for any potential transient species involved. Glycosylation yields, either with TFE or with MFE, were improved in the presence of the pyrene platform (Figure 5a and S20). On the contrary, the α/β stereoselectivity of these processes, already marginal for the reference compounds (2:1 and 1:2 with TFE and MFE, respectively) was further reduced in these cases. Interestingly, competition experiments monitored by HSQC spectra showed that this effect relies on a substantial acceleration in the production of the minor anomer, regardless of their stereochemistry or the alcohol employed in each case. That is, while the presence of the pyrene moiety significantly accelerates the formation of the β-linked product with TFE (**26β** vs **28β**), it promotes the same effect but for the α-anomer with MFE (**27α** vs **29α**. Figure 5a).

Regarding glycosylations with TFE, the presence of well resolved ^{1}H NMR signals for reagents and products prompted us to carry out additional experiments to monitor the individual reaction kinetics through sequential low-temperature 1D-NMR experiments. The representative time courses

independently obtained from the evolution of **16** and **17** are shown in Figure 5c, along with the relative initial reaction rates. The analysis of these data revealed a modest 2-fold increase for the formation rate of the α-anomer (**26α**), and a concomitant 4-fold increase for the β-anomer (**26β**), thus equating both formation rates and explaining the observed 1:1 stereoselectivity. Overall, the glycosylation reaction is 3-fold faster (α + β products) in the presence of the pyrene platform (Figure 5b, bar chart).

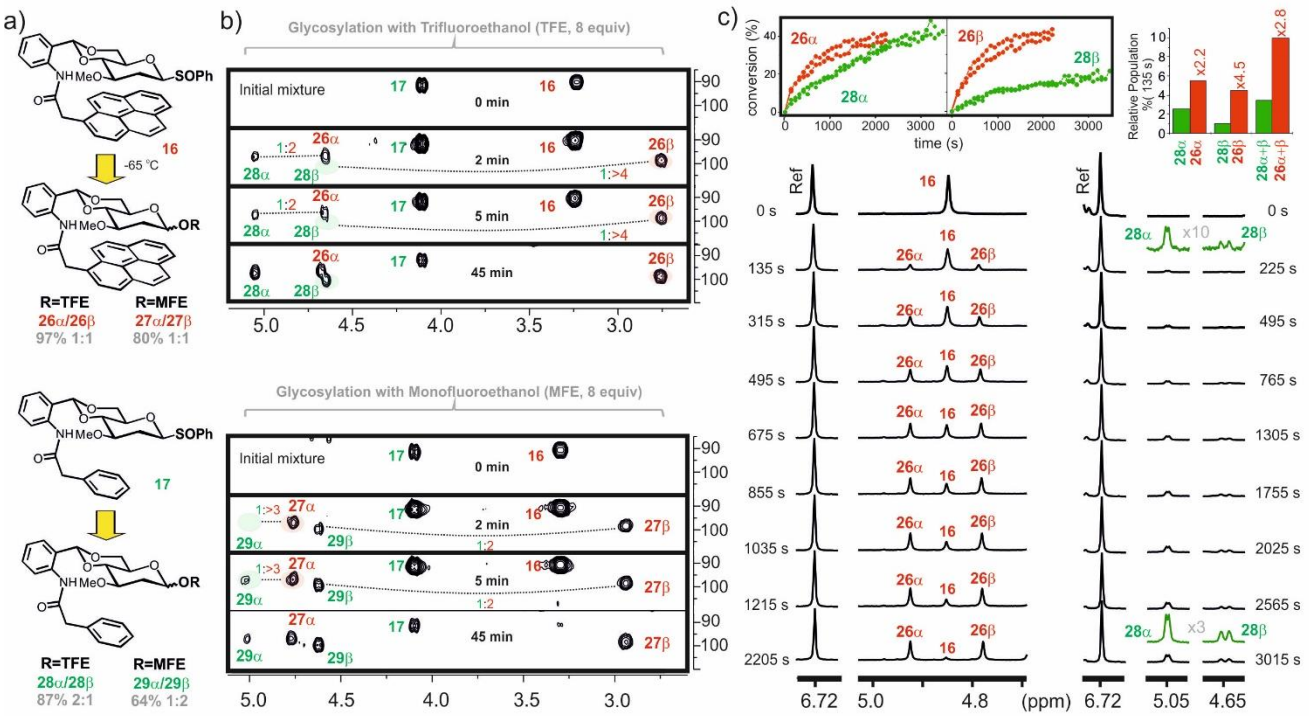

Figure 5.- *Family II. The 2-deoxy-glucose case. a) Reactions with **16** (up) and **17** (down) at -65 °C employing TFE or MFE. Yields and stereoselectivities are shown. b) Competition experiments with equimolecular ^{13}C-labeled **16**/**17** mixtures with TFE and MFE monitored by HSQCs. Data sets measured at different reaction times are displayed. Intensity ratios for the reaction products are indicated. c) Reactions performed either with **16** (left) or **17** (right) employing TFE, monitored through sequential 1D-NMR experiments at -65 °C. Kinetics of formation for the corresponding α and β products, derived from two independent experiments, are superimposed above. Bar chart represents the relative populations for the corresponding products at short reaction times.*

Encouraged by these promising results, we decided to push these latter models one step further into the S_N1 realm by the incorporation of a second pyrene moiety. To our delight, unprecedented shieldings (with ^{1}H NMR signals appearing with negative chemical shifts up to δ_H= -1.3 ppm) were induced by this optimized covalent scaffold for **18** and its corresponding glycosylation products **30 α/β** (Figure 6a). Of note, MD simulations showed that this effect results from the additive influence of both aromatic platforms, but does not imply a significantly tighter, more rigid geometry of the CH/π complex.

Reactions of both **18** and the reference derivative **19** with TFE yielded the final glycosylation products (**30 α/β** and **31 α/β**) with identical yields (in the 70-80% range) and stereoselectivities (1:2).

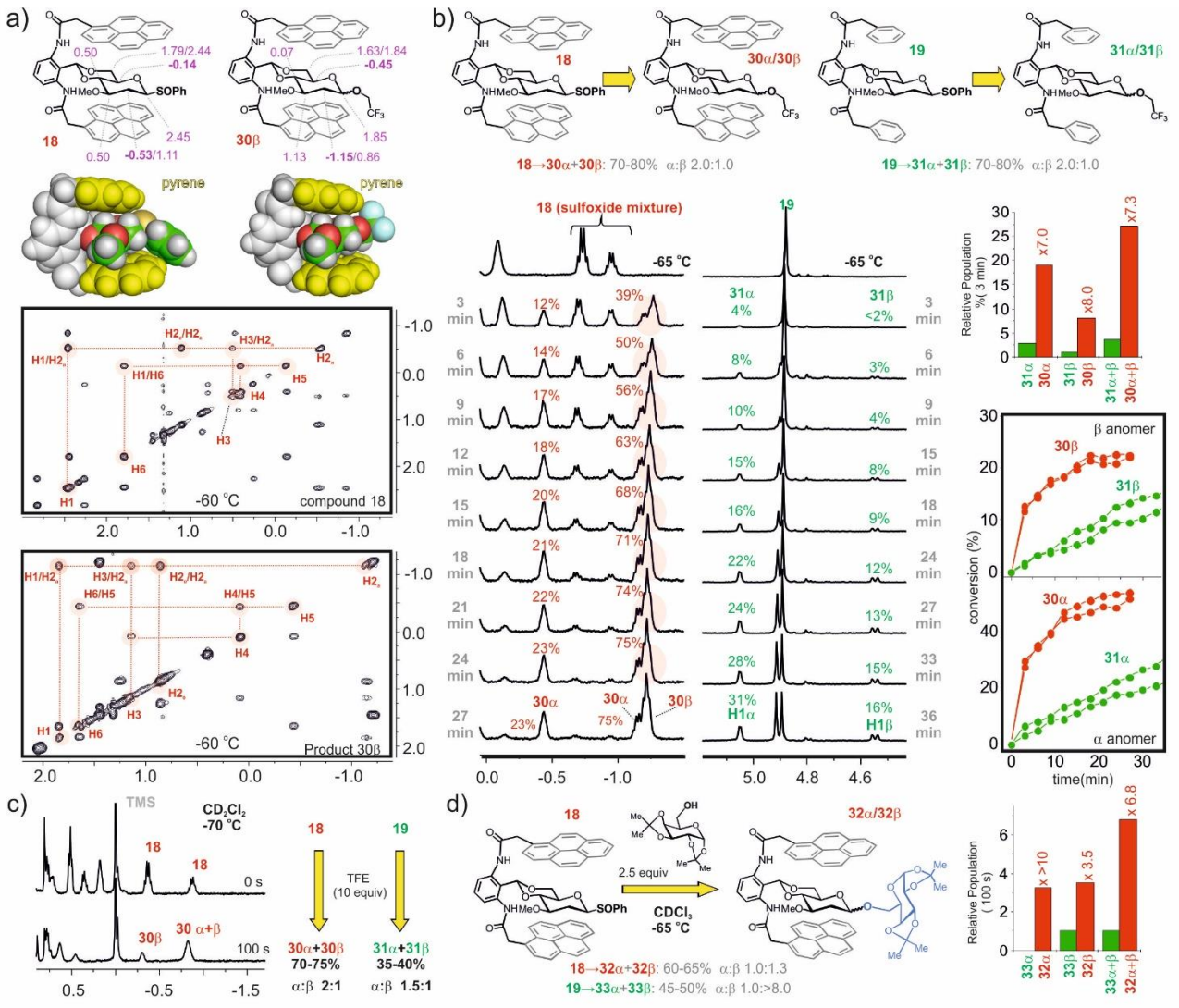

Figure 6.- *Family II. The 2-deoxy-glucose case. The influence of double stacking. a) Pyranose chemical shift perturbations measured for* ***18*** *and* ***30β*** *at -65 °C. CPK models for relevant conformations are shown below, together with the assigned COSY NMR experiments. b) The reactions of* ***18*** *(left, red) and* ***19*** *(right, green) with TFE were monitored by 1D-NMR experiments at -65 °C. Yields and stereoselectivities are displayed above. Formation kinetics of the corresponding α and β products are shown on the right. Bar chart represents the relative populations deduced for the glycosylation products at short reaction times. c) Assays carried out in CD_2Cl_2. For* ***18*** *the glycosylation was already complete in the first ^{1}H-NMR spectrum. Yields and stereoselectivities are indicated below. d) Reactions with* ***18*** *and* ***19*** *employing a synthetically relevant carbohydrate acceptor. Yields and stereoselectivities are displayed below. Bar chart represents the relative populations deduced for the glycosylation products at short reaction times.*

Satisfactorily, a careful monitorization of the glycosylation progress through sequential low-temperature 1D-NMR experiments was greatly facilitated by the presence of several proton signals with negative δ_H values. *Product conversions at the shortest reaction time tested (already showing a 40% evolution for* ***18****) were consistent with a 7-fold increase in the glycosylation rates for* ***30****α- and* ***30****β-anomers, as displayed in Figure 6b* (see also Figure S21). Moreover, these effects seem further noticeable in the presence of extremely poor *O*-nucleophiles, such as hexafluoroisopropanol (HFIP) (see Figure S22).

As expected, increasing the solvent dielectric from chloroform (ε=. 4.81) to dichloromethane (ε= 8.93) translates in faster glycosylation rates. However, reference model **19** still reacts significantly slower than the sandwiched donor **18** (whose reaction is now too fast to be followed by NMR. Figure 6c and S23). Of note, the acceleration observed for **18** is accompanied by a significant increase in the reaction yield.

Finally, models **18** and **19** were assayed in the context of a more conventional glycosylation reaction, employing the galactose acceptor shown in figure 6d (see also Figure S24). These experiments showed that the favorable influence exerted by aromatic platforms on the reaction rates are not limited to small, weakly nucleophilic alcohols but, to some extent, holds also for carbohydrate acceptors used in a slight stoichiometric excess. Interestingly, while reference derivative **19** reacts with significant stereoselectivity to yield a major β-glycosidation product, sandwiched donor **18** furnishes an almost equimolecular α:β mixture. According to these results, the employed galactose acceptor would react with reference **19** through a more associative process, probably involving an α-triflate intermediate, and with **18** in a more dissociative S_N1-like manner.

In summary, the combination of a 2-deoxy-glucopyranose donor with the appropriately positioned aromatic platforms has permitted, *for the first time, the observation of glycosylation rate enhancements associated to carbohydrate/aromatic interactions*.

DISCUSSION

The results described in the previous sections for families I and II reveal a stricking behavior, where the pyrene unit exerts a gradient of effects on the pyranose reactivity, ranging from significant inhibitions to moderate rate enhancements, as summarized in Figure 7. These data can be globally understood by considering the major driving forces that stabilize aromatic/carbohydrate complexes and how they evolve throughout the chemical reactions. On the one hand, the development of positive charge at the anomeric position reinforces attractive electrostatic interactions with the aromatic electronic quadrupole. This effect would be expected to be most significant under low dielectric environments and for highly dissociative S_N1-like processes. On the other hand, as the anomeric leaving group departs, the reactive pyranose distorts. In the simplest scenario, anomeric sp^3 to sp^2 rehybridation would imply that shape complementarity between the pyranose and the aromatic platform, optimal for a $^4C_1$ chair, is decreased, determining the disruption of at least one CH/π bond (the one involving the anomeric CH). Furthermore, for unconstrained pyranoses, more dramatic conformational changes could take place, thus leading to an overall deterioration of the van der Waals interactions with the aromatic platform. *According to this view, the net influence of aromatic stacking on the pyranose reactivity depends on a delicate balance between two conflicting energy contributions: electrostatic and van der Waals, favoring and opposing chemical evolution, respectively*.

Regarding family I models, they encompass an *unconstrained reactive* $^4C_1$ *pyranose* participating in strong CH/π interactions with the aromatic unit, in both the ground and activated (protonated) states. The experimentally observed decrease in reactivity for the carbohydrate/aromatic complexes indicates that the weakening of the van der Waals interactions at the transition state is not compensated by electrostatic forces. Indeed, CH/π and electrostatic contributions seem to be much more stabilizing for the activated species than for the distorted transition state, totalling in a net increase in the activation energy. This view is further supported by MD simulations (Figure 7a), which predict that a protonation of the anomeric substituent reinforces the CH/π bonds, leading to well-defined interaction pose, in agreement with the experimental chemical shift perturbations (Figure 2b). Significantly, the departure of the leaving group increases the internal

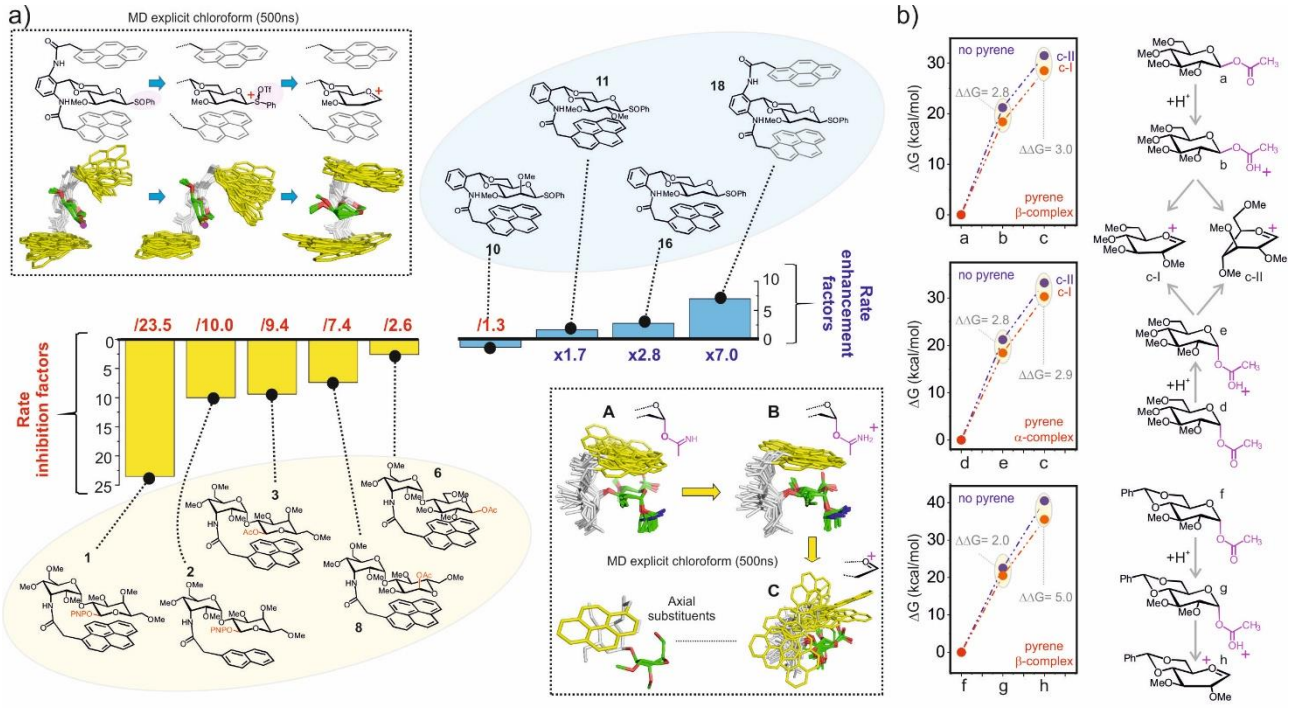

Figure 7.- a) *Summary of the results obtained for family I (left, yellow) and family II (right, cyan). The influence of the aromatic platform is expressed as rate inhibition (downwards) or enhancement (upwards) factors. Numeric values are shown in red and blue, respectively. Views of the conformational ensembles for the ground, activated and glycosyl cation states derived from solvated MD simulations (explicit $CHCl_3$) with a modified version of model* ***6*** *(bottom-right corner) and with* ***18*** *(top-left corner). b) Free energy penalty associated with the protonation of models* ***a***, ***d***, ***f*** *(top to bottom) and the subsequent glycosyl cation formation, in the presence (red) and absence (blue) of a complexed pyrene platform calculated by quantum mechanics with PCM/M06-2X/6-31g(d,p) in chloroform. The geometry of the complex (α or β) is also indicated. Net stabilizations promoted by the pyrene unit are expressed as ΔΔG (kcal/mol). The most stable conformations of the glycosyl cations were considered for the free and complexed states.*

mobility of the complex and frequent disruptions of the carbohydrate/aromatic contacts take place, due to the lack of an appropriate shape complementarity between the aromatic platform and the newly formed glycosyl cation. Indeed, the presence of axially oriented substituents in several of the conformational states of these species is not compatible with the geometric requirements for

establishing optimal CH/π interactions. On the contrary, for family II models, the presence of weaker, more dynamic CH/π bonds in the ground state *of the constrained pyranose analogues* determine their distinct behavior. Three common trends are apparent from the obtained data: first, the larger the S_N1 character of the reaction, the more favorable the influence exerted by the aromatic platform. Accordingly, major enhancements in the glycosylation rates are observed only for 2-deoxy-gluco-donors. Second, the conformational restriction imposed on the donor pyranose allows for a more optimized glycosyl cation/aromatic complex, as deduced by the analysis of the MD simulations (Figure 7a). Three, despite the improved shape complementarity between the pyrene unit and the nascent glycosyl oxocarbenium intermediate/transition state, the interactions are still highly mobile. Thus, the aromatic system provides a nurturing, more polar local environment for the developing pyranose charge, rather than fixing a preferred geometry of the complex, which translates into rate enhancements that are not accompanied by any particular stereocontrol. For example, for **18** no variation in the stereoselectivity of the reaction was detected with respect to reference model **19** when TFE was used as an acceptor (Figure 6a,b). On the contrary, the bulkier, more nucleophilic diacetone galactose yielded an opposite outcome (Figure 6d and S24): a preferential increase in the formation rate of the minor anomer, which determines a reduction in the reaction stereoselectivity. A similar behavior was also observed for donors **10**, **11** and **16**, which overall can be interpreted in terms of a *shift in the reaction mechanism toward a more dissociative S_N1-like process*. Interestingly, rate accelerations do come with moderate-to-significant improvements in the reaction yields for most analyzed derivatives (for example, **11** vs **14** or **15,** or models **16** vs **17**). This effect is clearly observable in the reaction of pair **18**/**19** with TFE in dichloromethane (Figure 6c and S23) and suggests that the aromatic platforms exert a certain protective influence, limiting the negative impact of undesired parasitic reactions on the glycosylation outcome. Consistently, we have also shown that these trends are maintained in other solvents, or mixtures of solvents with ranging polarities (Figure S23).

In summary, while the presence of aromatic quadrupole platforms facilitates the formation of glycosyl cations by electrostatic forces, pyranose distortion is detrimental for the establishment of proper CH/π contacts. Significantly, quantum mechanics calculations (PCM/M06-2X/6-31g(d,p) in chloroform) performed with simplified 1-*O*-acetyl model glycosides (Figure 7b), either constrained (**f**) or unconstrained (**a** and **d**), predict an enhanced stabilization of the glycosyl cation by the pyrene unit in the former complex **f** (ΔΔG of 5 kcal/mol vs 2.9-3.0 kcal/mol), in accordance with our experimental observations. Nevertheless, the theoretical stabilizations are, in all cases, overestimated, which might reflect the limitations inherent to these theoretical methods (implicit solvation, simplified intermolecular model complexes, absence of triflate counterions).

Overall, these data show that aromatic stacking promotes and facilitates S_N1 anomeric substitutions with all the expected consequences from a synthetic perspective. The fundamental

information derived from our studies could now be extrapolated to a more general chemical or enzymatic context. Hence, while measured accelerations are moderate, much larger enhancements would conceivably result from the additive influence of several, properly positioned aromatic platforms. According to our data, geometrical considerations are key to this goal. In particular, conventional parallel stacking leads to conflicting electrostatic and van der Waals contributions into the activation energy, which can limit or even, overturn the favorable influence exerted by the aromatic platform. Alternative stacking geometries, either lateral or parallel-shifted, could alleviate this conflict. This view is also supported by the unusual stacking modes observed in the active site of several glycosidases in complex with ligands or inhibitors (pdb codes 3WY4 or 2J77. Figure S25), which usually involve the formation of only one or two CH/π bonds per aromatic interaction, in contrast with the typical parallel stacking geometries (fully involving either the α– or β- face of the interacting pyranose) that take place in lectins and CBMs. This phenotypic recurring feature probably reflects the need to maintain the sugar ring relatively unconstrained by the aromatic residue, allowing the penalty-free pyranose distortions required for the reaction to proceed. Interestingly, quantum mechanics calculations performed on a simplified inhibitor/active site complex strongly suggest that interacting aromatic side-chains also contribute to stabilize the substrate positive charge, while keeping the active site free of water molecules (Figure S26).

It is worth mentioning that conflicting electrostatic and dispersive contributions to the activation energy could also be tilted in favor of the former by the incorporation of electron-donating substituents on the aromatic platform, which provides an alternative strategy to further reduce the transition state energy. Accordingly, previous studies by our group have shown that this modification indeed enhances carbohydrate/aromatic electrostatic forces, while having a lesser influence on the dispersive component of the stacking complexes.[5a] Carefully designed systems based on these concepts might eventually lead to the development of synthetic carbohydrate receptors with catalytic properties or engineered enzymes carrying unnatural aminoacids.

In view of the results presented in this work, aromatic moieties can indeed contribute to the catalysis of highly dissociative anomeric substitutions, provided that the electrostatics outcompete the van der Waals contributions to the activation energy.

CONCLUSIONS

While the participation of aromatic platforms in the molecular recognition of carbohydrates is undeniable, its potential involvement in catalysis remains an open question. In the work presented herein, we have tackled this issue by answering a simple question of fundamental relevance in glycoscience: can glycosyl cations be stabilized by aromatic platforms? Accordingly, we have dissected, in a systematic and extensive manner, the influence exerted by aromatic stacking on glycosylation or glycoside solvolysis reactions, whereby the potential of aromatic platforms as key

elements to sense and stabilize transient positive charge development was evaluated. The results derived from our study provide an affirmative answer to the aforementioned question: *aromatic platforms can indeed accelerate and improve SN1-like glycosylations, presumably by stabilizing positively charged transition states through cation/π interactions.* The obtained data also lent some meaningful insight into the nature of glycosyl cation/aromatic interaction and its influence on glycosylations. First, the glycosylations with 2-deoxy-donors, even in highly apolar environments and at very low temperatures, must involve highly cationic transition states, whereas glucose and mannose derivatives seem to proceed through either close ion pairs or highly reactive covalent intermediates. Secondly, glycosyl cation/aromatic interactions tend to be highly dynamic, thus reflecting the lack of a proper shape complementarity between both species. As a consequence, for flexible systems, they can exert a negligible influence on the stereoselectivity of the process. For more associative processes, the ability of aromatic units to selectively hinder bi-molecular substitutions, while still promoting the development of positive charge at the anomeric center, seems to determine a shift in the reaction mechanism towards the SN1, which has a concomitant negative impact on the overall stereoselectivity. This effect is especially clear when using bulky/nucleophilic acceptors and it is maintained for alternative solvents.

Finally, glycoside/aromatic complexes stabilized by strong CH/π interactions already present in the ground state can indeed undergo SN1-like reactions, such as solvolysis, with a greatly improved stereoselective outcome. Yet, this effect is accompanied by an increase in the activation energy of the process, which translates into a slower reaction rate, as exemplified by the methanolysis of model system **1**.

To the best of our knowledge, this represents the first experimental study on the influence of cation/π interactions in the formation and cleavage of glycosidic linkages, whose potential implications branch out into general catalysis and CAZyme engineering.

METHODS

A detailed description of the experimental and synthetic protocols together with the characterization of products and intermediates is included in the supplementary material.

SUPPLEMENTARY MATERIALS

A detailed description of the experimental methods and synthetic protocols together with the characterization of products and intermediates. Figures S1-S26 showing details of the NMR and reactivity experiments.

ACKNOWLEDGMENTS

This investigation was supported by research grants of the Spanish "Plan Nacional" CTQ2016-79255-P/CTQ2015-66702-R and the Mizutani Foundation for Glycoscience 17-0045. A.G.S acknowledges the Ministerio de Ciencia, Innovación y Universidades for a Juan de la Cierva incorporation contract. L. M-J thanks Ministerio de Economia y Competitividad for a FPI contract (BES-2014-070232).

REFERENCES

1.- a) Asensio, J.L.; Ardá, A.; Cañada, F.J.; Jiménez-Barbero, J. Carbohydrate-Aromatic Interactions. *Acc. Chem. Res.* **2013**, *46*, 946-954. b) Terraneo, G.; Potenza, D.; Canales, A.; Jiménez-Barbero, J.; Baldridge, K.K.; Bernardi, A. A Simple Model System for the Study of Carbohydrate−Aromatic Interactions. *J. Am. Chem. Soc.* **2007**, *129*, 2890-2900. (c) Fernández-Alonso, M.C.; Cañada, F.J.; Jimenez-Barbero, J.; Cuevas, G. Molecular Recognition of Saccharides by Proteins. Insights on the Origin of the Carbohydrate−Aromatic Interactions. *J. Am. Chem. Soc.* **2005**, *127*, 7379-7386. (d) Ramírez-Gualito, K.; Alonso-Ríos, R.; Quiroz-García, B.; Rojas-Aguilar, A.; Díaz, D.; Jiménez-Barbero, J.; Cuevas, G. Enthalpic Nature of the CH/π Interaction Involved in the Recognition of Carbohydrates by Aromatic Compounds, Confirmed by a Novel Interplay of NMR, Calorimetry, and Theoretical Calculations. *J. Am. Chem. Soc.* **2009**, *131*, 18129-18138. (e) Chavez, M.; Andreu, C.; Vidal, P.; Aboitiz, N.; Freire, F.; Groves, P.; Asensio, J.L.; Asensio, G.; Muraki, M.; Cañada, F.J.; Jimenez-Barbero, J. On the Importance of Carbohydrate–Aromatic Interactions for the Molecular Recognition of Oligosaccharides by Proteins: NMR Studies of the Structure and Binding Affinity of AcAMP2-like Peptides with Non-Natural Naphthyl and Fluoroaromatic Residues. *Chem.-Eur. J.* **2005**, *11*,7060-7074.

2.- a) Phillips, D. C. The hen hegg-white lysozyme molecule. *Proc. Nat. Acad. Sci. USA* **1967**, *57*, 483-495. b) Glickson, J.D.; Phillips, W.D.; Rupley, J.A. Proton magnetic resonance study of the indole NH resonances of lysozyme. Assignment, deuterium exchange kinetics, and inhibitor binding. *J. Am. Chem. Soc.* **1971**, *93*, 4031-4035. c) Quiocho, F.A. Carbohydrate-binding proteins-tertiary structures and protein-sugar interactions. *Ann. Rev. Biochem.* **1986**, *55*, 287-315. d) Lutteke, T.; Frank, M.; von der Lieth, C.W. Carbohydrate Structure Suite (CSS): analysis of carbohydrate 3D structures derived from the PDB. *Nucl. Acids Res.* **2005**, *33*, D242-D246.

3.- a) Tromans, R.A.; Carter, T.S.; Cabanne, L.; Crump, M.P.; Li, H.; Matlock, J.V.; Orchard, M.G.; Davis, A.P. A biomimetic receptor for glucose. *Nat. Chem.* **2019**, *11*, 52-56. b) Rios, P.; Mooibroek, T.J.; Carter, T.S.; William, C.; Wilson, M.R.; Crump, M.P.; Davis, A. P. Enantioselective carbohydrate recognition by synthetic lectins in water. *Chem. Sci.* **2017**, *5*, 4056-4061. c) Rios, P.; Carter, T.S.; Mooibroek, T.J.; Crump, M.P.; Lisbjerg, M.; Pittelkow, M.; Superkar, N.T.; Boons, G.J.; Davis, A. P. Synthetic Receptors for the High-Affinity Recognition of O-GlcNAc Derivatives. *Angew. Chem. Int. Ed.* **2016**, *55*, 3387-3392. d) Mooibroek, T.J.; Casas-Solvas, J.M.; Harniman, R.L.; Renney, C.M.; Carter, T.S.; Crump, M.P.; Davis, A.P. A threading receptor for polysaccharides. *Nat. Chem.* **2016**, *8*, 69-74. e) Ke, C.; Destecroix, H.; Crump, M.P. Davis, A.P. A simple and accessible synthetic lectin for glucose recognition and sensing. *Nat. Chem.* **2012**, *4*, 718-723. f) Davis, A.P. Supramolecular chemistry: Sticking to sugars. *Nature* **2010**, *464*, 169-170. g) Ferrand, Y.; Crump, M.P.; Davis, A.P. A synthetic lectin analog for biomimetic disaccharide recognition. *Science* **2007**, *318*, 619-622.

4.- a) Hudson, K.L.; Bartlett, G.J.; Diehl, R.C.; Agirre, J.; Gallagher, T.; Kiessling, L.L. Carbohydrate–Aromatic Interactions in Proteins. *J. Am. Chem. Soc.* **2015**, *137*, 15152-15116. b) Laughrey, Z.R.; Kiehna, S.E.; Riemen, A.J.; Waters, M.L. Carbohydrate−π Interactions: What Are They Worth?. *J. Am. Chem. Soc.*, **2008**, *130*, 14625-14633. c) Kiehna, S.E.; Laughrey, Z.R.; Waters, M.L. Evaluation of a carbohydrate-π interaction in a peptide model system. *Chem. Commun.*, **2007**, *39*, 4026-4028. d) Che-Hsiung, H.; Park, S.; Mortenson, D.E.; Foley, B.L.; Wang, X.; Woods, R.J.; Case, D.A.; Powers, E.T.; Wong, C.H.; Dyson, H.J.; Kelly, J.W. The Dependence of Carbohydrate-

Aromatic Interaction Strengths on the Structure of the Carbohydrate. *J. Am. Chem. Soc.* **2016**, *138*, 7636-7648.

5.- a) Jiménez-Moreno, E.; Jiménez-Osés, G.; Gómez, A.M.; Santana, A.G.; Corzana, F.; Bastida, A.; Jiménez-Barbero, J.; Asensio, J.L. A thorough experimental study of CH/π interactions in water: quantitative structure-stability relationships for carbohydrate/aromatic complexes. *Chemical Science* **2015**, *6*, 11, 6076-6085. b) Jiménez-Moreno, E.; Gómez, A.M.; Bastida, A.; Corzana, F.; Jiménez-Oses, G.; Jiménez-Barbero, J.; Asensio, J.L. Modulating weak interactions for molecular recognition: A dynamic combinatorial analysis for assessing the contribution of electrostatics to the stability of CH-π bonds in water. *Angew. Chem. Int. Edit.* **2015**, *54*, 4344-4348. c) Santana, A.G.; Jiménez-Moreno, E.; Gómez, A.M.; Corzana, F.; González, C.; Jiménez-Oses, G.; Jiménez-Barbero, J.; Asensio, J.L. A dynamic combinatorial approach for the analysis of weak carbohydrate/aromatic complexes: Dissecting facial selectivity in CH/π stacking interactions. *J. Am. Chem. Soc.* **2013**, *135*, 3347-3350.

6.- a) Ma, J.C.; Dougherty, D.A. The cation-π interaction. *Chem. Rev.* **1997**, *97*, 1303-1324. b) Dougherty, D.A. Cation-π interactions in chemistry and biology: A new view of benzene, Phe, Tyr, and Trp. *Science* **1996**, *271*, 163-168.

7.- Neel, A.J.; Hilton, M.J.; Sigman, M.S.; Toste, F.D. Exploiting non-covalent π interactions for catalyst design. *Nature* **2017**, *543*, 636-646.

8.- a) Adero, P.O.; Amaraseka, H.; Wen, P.; Bohe, L.; Crich, D. The Experimental Evidence in Support of Glycosylation Mechanisms at the SN1-SN2 Interface. *Chem. Rev.* **2018**, *118*, 8242-8284. b) Adero, P.O.; Furukawa, T.; Huang, M.; Mukherjee, D.; Retailleau, P.; Bohé, L.; Crich, D. Cation clock reactions for the determination of relative reaction kinetics in glycosylation reactions: Applications to gluco- and mannopyranosyl sulfoxide and trichloroacetimidate type donors. *J. Am. Chem. Soc.* **2015**, *137*, 10336-10345. c) Huang, M.; Retailleau, P.; Bohé, L.; Crich, D. Cation clock permits distinction between the mechanisms of α- And β-O- and β-C-glycosylation in the mannopyranose series: Evidence for the existence of a mannopyranosyl oxocarbenium ion. *J. Am. Chem. Soc.* **2012**, *134*, 14746-14749. d) Huang, M.; Garrett, G.E.; Birlirakis, N.; Bohé, L.; Pratt, D.A.; Crich, D. Dissecting the mechanisms of a class of chemical glycosylation using primary ^{13}C kinetic isotope effects. *Nat. Chem.* **2012**, *4*, 663-667. e) Crich, D. Mechanism of a chemical glycosylation reaction. *Acc. Chem. Res.* **2010**, *43*, 1144-1153. f) Crich, D.; Chandrasekera, N.S. Mechanism of 4,6-O-benzylidene-directed β-mannosylation as determined by α-deuterium kinetic isotope effects. *Angew. Chem. Int. Ed.* **2004**, *43*, 5386-5389.

9.- a) Bennet, A.J.; Sinnot, M.L. Complete kinetic isotope effect description of transition states for acid-catalyzed hydrolyses of methyl .alpha.- and .beta.-glucopyranosides. *J. Am. Chem. Soc.* **1986**, *108*, 7287-7294. b) Namchuk, M.N.; McCarter, J.D.; Becalski, A.; Andrews, T.; Withers, S.G. The Role of Sugar Substituents in Glycoside Hydrolysis. *J. Am. Chem. Soc.* **2000**, *122*, 1270-1277. c) Chan, J.; Tang, A.; Bennet, A.J. A Stepwise Solvent-Promoted SNi Reaction of α-d-Glucopyranosyl Fluoride: Mechanistic Implications for Retaining Glycosyltransferases. *J. Am. Chem. Soc.* **2012**, *134*, 1212-1220. d) Beaver, M.G.; Buscagan, T.M.; Lavinda, O.; Woerpel, K.A. Stereoelectronic Model to Explain Highly Stereoselective Reactions of Seven-Membered-Ring Oxocarbenium-Ion Intermediates. *Angew. Chem. Int. Ed.* **2016**, *55*, 1816-1819. e) Smith, D.M.; Woerpel, K.A. Electrostatic interactions in cations and their importance in biology and chemistry. *Org. Biomol. Chem.* **2006**, *4*, 1195-1201. f) van Rijssel, E.R.; van Delft, P.; Lodder, G.; Overkleeft, H.S.; van der Marel, G.A.; Filippov, D.V.; Codée, J.D.C. Furanosyl oxocarbenium ion stability and stereoselectivity. *Angew. Chem. Int. Ed.* **2014**, *53*, 10381-10385. g) Ayala, L.; Lucero, C.G.; Romero, J.A.C.; Tabacco, S.A.; Woerpel, K.A. Stereochemistry of Nucleophilic Substitution Reactions Depending upon Substituent: Evidence for Electrostatic Stabilization of Pseudoaxial Conformers of Oxocarbenium Ions by Heteroatom Substituents. *J.Am. Chem. Soc.* **2003**, *125*, 15521-15528.

10.- a) Chatterjee, S.; Moos, S.; Hentschel, F.; Gilmore, K.; Seeberger, P.H. An Empirical Understanding of the Glycosylation Reaction. *J. Am. Chem. Soc.* **2018**, *140*, 11942-11953. b) Heuckendorff, M.; Bendix, J.; Pedersen, C.M.; Bols, M. β-selective mannosylation with a 4,6-silylene-tethered thiomannosyl donor. *Org. Lett.* **2014**, *16*, 1116-1119.

11.- Martin, A.; Arda, A.; Désiré, J.; Martin-Mingot, A.; Probst, N.; Sinaÿ, P.; Jiménez-Barbero, J.; Thibaudeau, S.; Blériot, Y. Catching elusive glycosyl cations in a condensed phase with HF/SbF_5 superacid. *Nat. Chem.* **2016**, *8*, 186-191.

12.- a) Mucha, E.; Marianski, M.; Xu, F.F.; Thomas, D.A.; Meijer, G.; von Helden, G.; Seeberger, P.H.; Pagel, K. Unravelling the structure of glycosyl cations via cold-ion infrared spectroscopy. *Nat. Commun.* **2018**, *9*, 1-5. b) Elferink, H.; Severijnen, M.E.; Martens, J.; Mensink, R.A.; Berden, G.; Oomens, J.; Rutjens, F.P.J.T.; Rijs, A.M.; Boltje, T.J. Direct Experimental Characterization of Glycosyl Cations by Infrared Ion Spectroscopy. *J. Am. Chem. Soc.* **2018**, *140*, 6034-6038.

13.- Lillelund, V.H.; Jensen, H.H.; Liang, X.; Bols, M. Recent Developments of Transition-State Analogue Glycosidase Inhibitors of Non-Natural Product Origin. *Chem. Rev.* **2002**, *102*, 515-553.

14.- a) Danby, P.M.; Withers, S.G. Glycosyl Cations versus Allylic Cations in Spontaneous and Enzymatic Hydrolysis. *J. Am. Chem. Soc.* **2017**, *139*, 10629-10632. b) Zechel, D.L.; Withers, S.G. Glycosidase Mechanisms: Anatomy of a Finely Tuned Catalyst. *Acc. Chem. Res.* **2000**, *33*, 11-18. c) Vasella, A.; Davies, G.J.; Bohm, M. Glycosidase mechanisms. *Curr. Opin. Chem. Biol.* **2002**, *6*, 619-629.

15.- a) Ren, W.; Pengelly, R.; Farren-Dai, M.; Shansi Kazem Abadi, S.; Oehler, V.; Akintola, O.; Draper, J.; Meanwell, M.; Chakladar, S.; Świderek, K; Moliner, V.; Britton, R.; Gloster, T.M.; Bennet, A.J. Revealing the mechanism for covalent inhibition of glycoside hydrolases by carbasugars at an atomic level. *Nat. Commun.* **2018**, *9*, 1-12. b) Shamsi Kazem Abadi, S.; Tran, M.; Yadav, A.K.; Adabala, P.J.P.; Chakladar, S.; Bennet, A.J. New Class of Glycoside Hydrolase Mechanism-Based Covalent Inhibitors: Glycosylation Transition State Conformations. *J. Am. Chem. Soc.* **2017**, *139*, 10625-10628.

16.- Nerinckx, W.; Desmet, T.; Claeyssens, M. A hydrophobic platform as a mechanistically relevant transition state stabilising factor appears to be present in the active centre of all glycoside hydrolases. *Febs. Lett.* **2003**, *538*, 1-7.

17.- Iglesias-Fernández. J.; Hanckock, S.M.; Lee, S.S.; Khan, M.; Kirkpatrick, J.; Oldham, N.J.; McAuley, K.; Fordham-Skelton, A.; Rovira, C.; Davis, B.G. A front-face 'SNi synthase' engineered from a retaining 'double-SN2' hydrolase. *Nat. Chem. Biol.* **2017**, *13*, 874-886.

18.- Vacas, T.; Corzana, F.; Jiménez-Osés, G.; González, C.; Gómez, A.M.; Bastida, A.; Revuelta, J.; Asensio, J.L. Role of aromatic rings in the molecular recognition of aminoglycoside antibiotics: Implications for drug design. *J. Am. Chem. Soc.* **2010**, *132*, 12074-12090.

19.- Lin, L.; Li, C.; Alexov, E. On the dielectric "constant" of proteins: Smooth dielectric function for macromolecular modeling and its implementation in DelPhi. *J. Chem. Theory Comput.* **2013**, *9*, 2126-2136.

20.- Crich, D.; Sun, S. Are glycosyl triflates intermediates in the sulfoxide glycosylation method? A chemical and ^{1}H, ^{13}C, and ^{19}F NMR spectroscopic investigation. *J. Am. Chem. Soc.* **1997**, *119*, 11217-11223.

21.- a) van der Vorm, S.; Hansen, T.; Overkleeft, H.S.; van der Marel, G.A.; Codée, J.D.C. The influence of acceptor nucleophilicity on the glycosylation reaction mechanism. *Chem. Sci.* **2017**, *8*, 1867-1875. b) van der Vorm, S.; van Hengst, J.M.A.; Bakker, M.; Overkleeft, H.S.; van der Marel, G.A.; Codée, J.D.C. Mapping the Relationship between Glycosyl Acceptor Reactivity and Glycosylation Stereoselectivity. *Angew. Chem. Int. Ed.* **2018**, *57*, 8240-8244.

22.-Reactivity assays, were carried out with enantiomerically pure sulfoxides unless explicitly stated. This structural parameter was shown to have no influence on the obtained conclusions.

23.- Hon, D.; Taha, H.A.; Lowary, T.L. 2,3-Anhydrosugars in Glycoside Bond Synthesis: Mechanism of 2-Deoxy-2-thioaryl Glycoside Formation. *J. Am. Chem. Soc.* **2009**, *131*, 12937-12948.

24.- Kiyooka, S.I.; Kaneno, D.; Fujiyama, R. Intrinsic reactivity index as a single scale directed toward both electrophilicity and nucleophilicity using frontier molecular orbitals. *Tetrahedron* **2013**, *69*, 4247-4258.

25.-Bennet, C.S.; Galan, M.C. Methods for 2-Deoxyglycoside Synthesis. *Chem. Rev.* **2018**, *118*, 7931-7985.

TOC

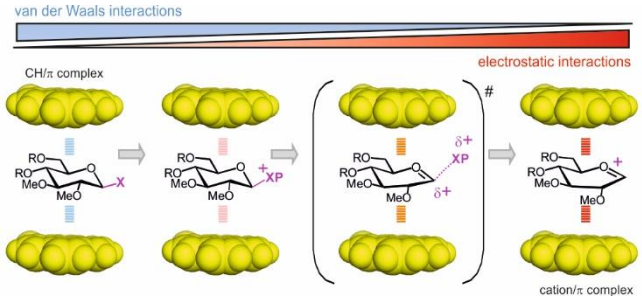
van der Waals interactions
electrostatic interactions
CH/π complex
RO
RO
MeO
MeO
X
XP
δ+
δ+
#
cation/π complex